Phosphoregulation of the intracellular termini of K^+-Cl^- cotransporter 2 (KCC2) enables flexible control of its activity

Received for publication, June 7, 2018, and in revised form, September 1, 2018 Published, Papers in Press, September 10, 2018, DOI 10.1074/jbc.RA118.004349

Antje Cordshagen[‡], Wiebke Busch[‡], Michael Winklhofer[§¶], Hans Gerd Nothwang[‡¶], and Anna-Maria Hartmann[‡¶1]

From the [‡]Neurogenetics group, Center of Excellence Hearing4all, School of Medicine and Health Sciences, [§]Institute for Biology and Environmental Sciences IBU, and [¶]Research Center for Neurosensory Sciences, Carl von Ossietzky University Oldenburg, 26111 Oldenburg, Germany

Edited by Mike Shipston

The pivotal role of K^+-Cl^- cotransporter 2 (KCC2) in inhibitory neurotransmission and severe human diseases fosters interest in understanding posttranslational regulatory mechanisms such as (de)phosphorylation. Here, the regulatory role of the five *bona fide* phosphosites Ser^{31}, Thr^{34}, Ser^{932}, Thr^{999}, and Thr^{1008} was investigated by the use of alanine and aspartate mutants. Tl^+-based flux analyses in HEK-293 cells demonstrated increased transport activity for S932D (mimicking phosphorylation) and T1008A (mimicking dephosphorylation), albeit to a different extent. Increased activity was due to changes in intrinsic activity, as it was not caused by increased cell-surface abundance. Substitutions of Ser^{31}, Thr^{34}, or Thr^{999} had no effect. Additionally, we show that the indirect actions of the known KCC2 activators staurosporine and *N*-ethylmaleimide (NEM) involved multiple phosphosites. S31D, T34A, S932A/D, T999A, or T1008A/D abrogated staurosporine mediated stimulation, and S31A, T34D, or S932D abolished NEM-mediated stimulation. This demonstrates for the first time differential effects of staurosporine and NEM on KCC2. In addition, the staurosporine-mediated effects involved both KCC2 phosphorylation and dephosphorylation with Ser^{932} and Thr^{1008} being *bona fide* target sites. In summary, our data reveal a complex phosphoregulation of KCC2 that provides the transporter with a toolbox for graded activity and integration of different signaling pathways.

K^+-Cl^- cotransporter 2 (KCC2)[2] plays a pivotal role in inhibitory neurotransmission. Under normal physiological conditions, KCC2 mediates outward transport of K^+ and Cl^-, thereby lowering the intracellular Cl^- concentration ($[Cl^-]_i$) in neurons (1–3). This renders the action of GABA or glycine hyperpolarizing as their receptors are ligand-coupled Cl^- channels. KCC2 exists in two isoforms, KCC2a and KCC2b, which differ in their N termini due to alternative promotors and first exon usage (4). In the adult, KCC2b is the most prominent isoform (5). Mice with disruption of the gene *Slc12a5* encoding both KCC2a and KCC2b die shortly after birth due to motor deficits (6). KCC2b-deficient mice survive up to 3 weeks postnatally (7), whereas KCC2a-deficient mice show no obvious phenotype (8).

Dysregulation of KCC2 is associated with several neurological and psychiatric disorders, including epilepsy, neuropathic pain, spasticity, ischemic insults, brain trauma, schizophrenia, and autism (9–19). This renders KCC2 a prime pharmacotherapeutic target and fosters interest in understanding posttranslational mechanisms of its regulation (20–25). Among those, phosphorelated mechanisms are most intensively scrutinized. The broad-spectrum kinase inhibitor staurosporine enhances KCC2 transport activity in hippocampal neurons (26). *N*-Ethylmaleimide (NEM) enhances KCC transport activity as well and is thought to act on the same regulatory kinases as staurosporine (27–30). In contrast, the protein phosphatase inhibitors calyculin and okadaic acid block KCC activation by cell swelling (31, 32).

Functional characterization of several KCC2 phosphosites demonstrated the importance of phosphorelated regulatory mechanisms (20, 23, 27, 33, 34). Dephosphorylation of the N-terminal phosphosite Thr^6 of KCC2a (35, 36) or the pan-C-terminal phosphosites Thr^{906} and Thr^{1006} (numbering according to mouse KCC2b) increases transport activity (27, 37–39). Similarly, phosphorylation of Tyr^{903} and Tyr^{1087} decreases cell-surface expression as well as transport activity of Tyr^{1087} (40–42). In contrast, phosphorylation of Thr^{934}, Ser^{937}, or Ser^{940} increases KCC2 transport activity (27, 43). The latter three phosphorylation sites are encoded in exon 22, which is exclusively conserved throughout vertebrate KCC2 and nontherian KCC4 (27, 33).

Analyses of the underlying regulatory mechanism identified several kinases that interact with KCC2. These kinases include protein kinase C (PKC), with-no-lysine (K) kinases (WNKs), oxidative stress–responsive kinase 1 (OSR1), Ste20p-related proline/alanine-rich kinase (SPAK), and creatine kinase (CKB) (35–37, 43–46). PKC was shown to phosphorylate Ser^{940} (43), and WNKs interact with SPAK/OSR1 to phosphorylate the KCC2a isoform–specific N-terminal residue Thr^6 and the pan-residue Thr^{1006} (35–37, 39, 47). WNKs also interact with a yet unknown kinase to phosphorylate Thr^{906} (36, 37, 39). Kinases

This work was supported by Deutsche Forschungsgemeinschaft Grants NO428/14-1 (to H. G. N.) and HA 6338/2-1 (to A.-M. H.). The authors declare that they have no conflicts of interest with the contents of this article.
This article contains Figs. S1 and S2.

[1] To whom correspondence should be addressed: Division of Neurogenetics, Carl von Ossietzky University Oldenburg, 26111 Oldenburg, Germany. Tel.: 49-441-798-2937; Fax: 49-441-798-5649, E-mail: anna.maria.hartmann@uol.de.

[2] The abbreviations used are: KCC, K^+-Cl^- cotransporter; NEM, *N*-ethylmaleimide; PKC, protein kinase C; WNK, with-no-lysine (K) kinase; OSR1, oxidative stress–responsive kinase 1; SPAK, Ste20p-related proline/alanine-rich kinase; HEK, human embryonic kidney; *mm*, *M. musculus*.

Table 1
Phosphosites in PhosphoSitePlus and PHOSIDA
Dashes indicate no presence in the data base or they were not publicized. *rn*, *R. norvegicus*.

PhosphoSitePlus *mm*KCC2	PhosphoSitePlus *rn*KCC2	PHOSIDA *mm*KCC2	Transport activity measured by (Ref.)
Thr^{6}	—	—	34–36
Ser^{25}	Ser^{25}	Ser^{25}	27, 34
Ser^{26}	Ser^{26}	Ser^{26}	27, 34
—	Ser^{31}	Ser^{31}	—
Thr^{34}	Thr^{34}	Thr^{34}	72
Thr^{906}	Thr^{906}	Thr^{906}	27, 37, 39
Ser^{913}	—	—	—
Ser^{932}	—	(Ser^{932})	—
Thr^{934}	Thr^{934}	(Thr^{934})	27
Ser^{937}	Ser^{937}	Ser^{937}	27
Ser^{940}	Ser^{940}	Ser^{940}	28, 43
Ser^{988}	—	—	—
Thr^{999}	—	—	—
Thr^{1006}	Thr^{1007}	Thr^{1006}	27, 28, 39
Thr^{1008}	—	Thr^{1008}	—
Ser^{1021}	Ser^{1022}	Ser^{1021}	27
Ser^{1024}	Ser^{1025}	(Ser^{1024})	27
Ser^{1025}	Ser^{1026}	Ser^{1025}	27

involved in the phosphorylation of the other phosphosites have yet to be identified. Overall, regulation of KCC2 transport activity by phosphorylation involves a variety of phosphosites as well as kinases and phosphatases. This complexity likely serves to match the demand for a fine-grained setting of $[Cl^-]$ to modulate inhibitory neurotransmission and to enable integration of different signaling pathways in neurons (27, 33, 34, 48–50).

Here, we analyzed the impact of *bona fide* phosphosites identified in large-scale phosphoproteomics studies on KCC2 transport activity. These residues were substituted by either alanine or aspartate in mouse KCC2b to block or mimic phosphorylation, respectively. Subsequently, transport activity measurements were performed in HEK-293 cells to determine KCC2 transport activity in the presence of various agents.

Results

Database mining and evolutionary conservation of KCC2 phosphosites

The databases PhosphoSitePlus and PHOSIDA subsume all experimentally observed phosphosites that were identified by MS-based proteomics studies (51, 52). Using KCC2 as query, we identified eight *bona fide* phosphosites, Ser^{31}, Thr^{34}, Ser^{913}, Ser^{932}, Ser^{988}, Thr^{999}, and Thr^{1008}, in addition to the previously described phosphosites Thr^{6}, Ser^{25}, Ser^{26}, Thr^{906}, Thr^{934}, Ser^{937}, Ser^{940}, Thr^{1006}, Ser^{1021}, Ser^{1024}, and Ser^{1025} (Table 1). Five of these eight phosphosites, Thr^{6}, Ser^{25}, Ser^{26}, Ser^{31}, and Thr^{34} are located in the cytoplasmic N terminus whereby Thr^{6} is contained in both alternative exons 1 of KCC2a and KCC2b and Ser^{25}, Ser^{26}, Ser^{31}, and Thr^{34} are shared by both isoforms. The remaining phosphosites are located in the shared C terminus of both KCC2 isoforms. In the following, we focus our analyses on the two N-terminal Ser^{31} and Thr^{34} and the three C-terminal Ser^{932}, Thr^{999}, and Thr^{1008} phosphosites as they were so far not characterized.

Multiple sequence alignment of vertebrate KCC subfamily members revealed that these phosphosites cover different patterns of phylogenetic conservation (Fig. 1). The phosphosite Thr^{1008} is highly conserved throughout all vertebrate KCC isoforms. Thr^{999} is moderately conserved throughout KCC2 and KCC3 and partially conserved in KCC1 and KCC4. The N-terminal phosphosite Ser^{31} is highly conserved in orthologous KCC2 members and is rarely observed in KCC1 and KCC4, whereas Thr^{34} is mainly present in therian KCC2. Ser^{932} is highly conserved in vertebrate KCC2 and nontherian KCC4. This phosphosite is located in exon 22, which also harbors the previously analyzed and highly conserved phosphosites Thr^{934}, Ser^{937}, and Ser^{940} (33).

Expression analyses of KCC2 phosphomutants

To study the posttranslational regulatory impact of phosphorylated Ser^{31}, Thr^{34}, Ser^{932}, Thr^{999}, and Thr^{1008} for KCC2b (*Mus musculus* (*mm*)KCC2b) function, we generated two mutants for each phosphosite mimicking the phosphorylated (mutation into aspartate) or dephosphorylated (mutation into alanine) status. This resulted in a total of 10 mutants ($KCC2^{S31A/D}$, $KCC2^{T34A/D}$, $KCC2^{S932A/D}$, $KCC2^{T999A/D}$, and $KCC2^{T1008A/D}$). To analyze whether these mutations affect the expression pattern of KCC2, the constructs were transiently expressed in HEK-293 cells. All mutants showed a transfection rate in HEK-293 cells similar to $KCC2^{WT}$ (Fig. S1). Furthermore, immunoreactivity against all mutants was detected at the plasma membrane and in the cytosol (Fig. 2). Only the nucleus was spared. Thus, all mutants were well expressed in HEK-293 cells and therefore suitable for transport activity measurements.

Regulatory role of S932D and T1008A

To investigate the regulatory relevance of the five *bona fide* phosphosites, we determined the transport activity of phosphomimetic (aspartate) and dephosphomimetic (alanine) mutations of *mm*KCC2 by Tl^+ flux measurements. All mutants as well as the $KCC2^{WT}$ displayed at least a 2.9-times increased transport activity compared with mock-transfected cells (Fig. 3, Table 2, and Fig. S2). The loop diuretic furosemide, which specifically inhibits the function of cation-chloride cotransporters (53, 54), blocks most of the flux, demonstrating that the transport activity was largely mediated by KCC2 (see Fig. 5, Table 2, and Fig. S2).

Analogous to the previously described N-terminal Ser^{25} and Ser^{26} phosphosites (27), substitution of Ser^{31} and Thr^{34} by alanine or aspartate did not alter transport activity compared with $KCC2^{WT}$. Similar results were obtained for the C-terminal mutants S932A, T999A/D, and T1008D. All four mutants showed a transport activity indistinguishable from $KCC2^{WT}$ (Fig. 3 and Table 2). In contrast, substitution of Ser^{932} by aspartate and Thr^{1008} by alanine significantly enhanced KCC2 transport activity, albeit to a different extent (Fig. 3 and Table 2). To conclude, phosphorylation of the C-terminal residue Ser^{932} and dephosphorylation of Thr^{1008} result in an increased KCC2 transport activity in HEK-293 cells.

No change in abundance and cell-surface expression of $KCC2^{S932D}$ and $KCC2^{T1008A}$

To analyze whether the enhanced activity of the two phosphomutants is due to increased abundance at the cell surface, we performed biotinylation assays for $KCC2^{WT}$, S932D, and T1008A (Fig. 4). $KCC2^{WT}$ displayed a cell-surface localization of 16.7 ± 1.6% compared with the total KCC2 protein amount.

N-terminus					C-terminus															
[*mm*KCC2b]	31			34	932								940	999						1008
*hs*KCC1	P	L	E	A										V	G	A	D	K	I	Q	M	T	W	T
*rn*KCC1	P	L	D	A										V	G	A	D	K	I	Q	M	T	W	T
*md*KCC1	C	S	E	A										A	R	P	E	K	V	Q	M	T	W	T
*ac*KCC1	N	T	D	S										T	I	P	E	K	I	Q	M	T	W	T
*gg*KCC1	S	S	E	A										T	V	P	E	N	I	Q	M	T	W	T
*tg*KCC1	S	S	E	A										P	V	P	E	N	I	Q	M	T	W	T
*xt*KCC1	G	S	E	A										L	E	L	A	K	I	H	M	T	W	T
*tr*KCC1	G	A	D	G										L	P	S	E	K	V	Q	M	T	W	T
*dr*KCC1	S	S	D	A										I	L	P	E	K	N	Q	M	T	W	T
*hs*KCC3	N	S	N	Y										T	Y	Q	E	K	V	H	M	T	W	T
*rn*KCC3	N	S	N	Y										T	Y	Q	E	K	V	H	M	T	W	T
*md*KCC3	N	S	N	F										T	Y	Q	E	K	V	H	M	T	W	T
*ac*KCC3	N	I	N	Y										T	Y	Q	E	K	V	H	M	T	W	T
*xt*KCC3	H	T	D											A	V	P	D	R	V	H	M	T	W	T
*tr*KCC3	N	T	H	V										E	H	H	R	R	V	Q	M	T	W	T
*hs*KCC2	S	T	D	T	S	I	T	D	E	S	R	G	S	T	D	P	E	K	V	H	L	T	W	T
*rn*KCC2	S	T	D	T	S	I	T	D	E	S	R	G	S	T	D	P	E	K	V	H	L	T	W	T
*mm*KCC2	S	T	D	T	S	I	T	D	E	S	R	G	S	T	D	P	E		V	H	L	T	W	T
*md*KCC2	S	T	D	S	S	I	T	D	E	S	R	G	S	A	A	P	E	K	V	H	L	T	W	T
*ac*KCC2					S	I	T	D	E	S	R	G	S	A	A	P	E	K	V	H	L	T	W	T
*gg*KCC2	S	T	D	L	S	I	T	D	E	S	R	G	S	S	A	P	E	K	V	H	L	T	W	T
*xt*KCC2	S	S	E	M	S	I	T	D	E	S	R	G	S	T	T	Q	E	K	V	H	L	T	W	T
*tg*KCC2					S	I	T	D	E	S	R	G	S	A	A	P	E	K	V	H	L	T	W	T
*dr*KCC2_1	D	H	D		S	I	T	D	E	S	R	I	S	P	T	S	D	R	V	H	M	T	W	T
*dr*KCC2_2	S	T	D		S	I	T	D	S	S	R	G	S	T	P	G	T	A	V	Q	M	T	W	S
*hs*KCC4	N	V	E	V										P	T	P	D	K	V	Q	M	T	W	T
*rn*KCC4	N	V	E	V										P	T	P	D	K	V	Q	M	T	W	T
*md*KCC4	N	T	D	M	S	I	S	N	E	S	R	C	S	A	T	P	E	K	V	Q	M	T	W	T
*ac*KCC4	N	A	S	M	S	I	S	D	E	S	R	S	S	T	T	P	E	K	V	Q	M	T	W	T
*gg*KCC4	S	A	E	M	S	I	T	D	E	S	R	G	S	A	M	P	E	K	V	Q	M	T	W	T
*tg*KCC4	C	A	E	L	S	I	T	D	E	S	R	G	S	A	V	P	E	K	V	Q	M	T	W	T
*dr*KCC4_1	S	T	S	V	S	I	T	D	V	S	R	G	S		A	P	T		P	A	T	M	S
*dr*KCC4_2	N	T	D	D	S	I	T	D	E	S	R	S	S	A	T	P	E	R	V	H	M	T	W	T

Figure 1. Evolutionary conservation of phosphosites and their neighboring amino acids in KCC subgroups. Ser[31], Thr[34], and Thr[999] are moderately conserved in vertebrate KCC subfamily members. The phosphosites Thr[1006] and Thr[1008] are highly conserved throughout vertebrate KCCs. Ser[932], Ser[937], Thr[934], and Ser[940] display similar degrees of phylogenetic conservation. They are only present in vertebrate KCC2 and in nontherian KCC4. *hs*, *H. sapiens*; *rn*, *Rattus norvegicus*; *md*, *Monodelphis domestica*; *gg*, *Gallus gallus*; *tg*, *Taeniopygia guttata*; *ac*, *Anolis carolinensis*; *xt*, *Xenopus tropicalis*; *tr*, *Takifugu rubripes*; *Dr*, *Danio rerio*.

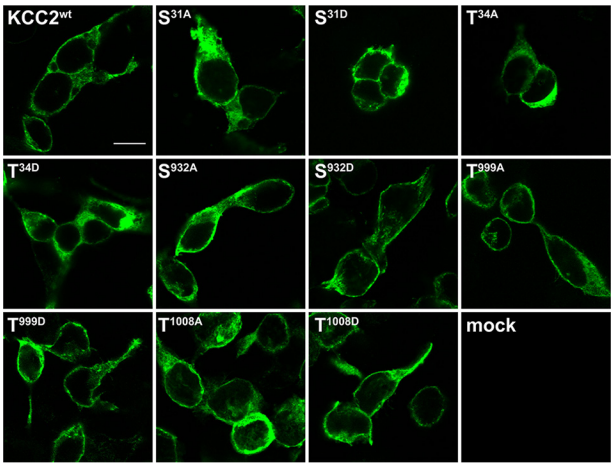

Figure 2. Expression of KCC2[WT] or KCC2 phosphomutants in HEK-293 cells. The subcellular distribution of KCC2 mutants was indistinguishable from KCC2[WT] with immunoreactivity outside the nucleus. Photomicrographs were taken with a confocal laser-scanning microscope. *Scale bar*, 10 μm.

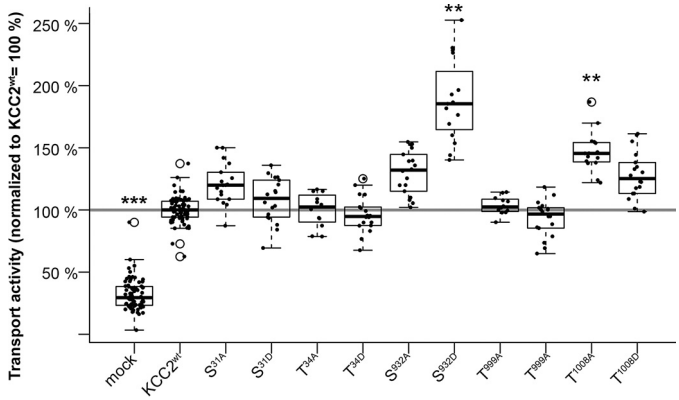

Figure 3. Transport activity of KCC2 phosphomutants. HEK-293 cells were transfected with KCC2[WT] or KCC2 phosphomutant constructs. Transport activity was determined by performing Tl^+ flux measurements. The Tl^+ flux determined for KCC2[S31A/D], KCC2[T34A/D], KCC2[S932A], KCC2[T999A/D], and KCC2[T1008D] was similar to the flux of KCC2[WT]. In contrast, KCC2[S932D] and KCC2[T1008A] mutants resulted in significantly increased transport activity. The graph represents the data of at least four independent measurements (each consisting of three technical replicates) normalized to KCC2[WT]. Statistical analysis is presented in Table 2 (**, $p < 0.01$; ***, $p < 0.001$). *Circles* indicate outliers with respect to the 1.5 × interquartile range of the box plot. *Error bars* represent S.E.

This is in line with previously published results that reported a 12–13% surface localization for rat KCC2 (55, 56). The cell-surface rates of S932D (19.8 ± 2.5%) and T1008A (17.4 ± 0.2%) were indistinguishable from KCC2[WT]. Thus, the enhanced

Table 2
Transport activity under basal conditions and in the presence of furosemide
**, $p < 0.01$; ***, $p < 0.001$; n.s., not significant.

	Basal conditions (significance in comparison with $KCC2^{WT}$)	2 mM furosemide (significance in comparison with untreated samples)
	%	%
Mock	32 ±2 (***)	27 ±2 (n.s.)
$KCC2^{WT}$	100 ±2 (n.s.)	27 ±1 (***)
S31A	121 ±7 (n.s.)	45 ±7 (***)
S31D	108 ±7 (n.s.)	32 ±4 (***)
T34A	100 ±7 (n.s.)	27 ±2 (***)
T34D	96 ±6 (n.s.)	37 ±4 (***)
S932A	130 ±7 (n.s.)	24 ±3 (***)
S932D	188 ±15 (**)	27 ±3 (***)
T999A	104 ±4 (n.s.)	24 ±2 (***)
T999D	93 ±6 (n.s.)	26 ±2 (***)
T1008A	147 ±7 (**)	27 ±4 (***)
T1008D	128 ±8 (n.s.)	23 ±2 (***)

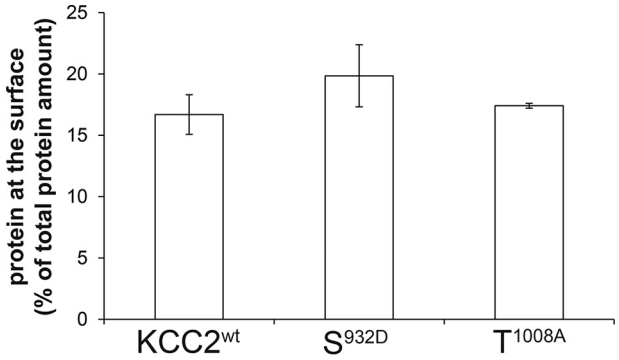

Figure 4. Cell-surface expression of KCC2 phosphomutants. The cell-surface amount of the indicated KCC2 mutants was quantitatively determined by immunoblot analysis. $KCC2^{WT}$ and the KCC2 mutants S932A or T1008A show similar abundance at the surface. The plot depicts the mean of at least three experiments ±S.E. (*error bars*).

transport activity of S932D and T1008A is caused by intrinsically kinetic effects and not by changes in KCC2 cell-surface abundance.

Staurosporine and NEM differentially affect KCC2 phosphomutants

Staurosporine is a broad kinase inhibitor that generally activates KCCs (27, 57, 58). To investigate whether Ser^{31}, Thr^{34}, Ser^{728}, Ser^{932}, Thr^{999}, or Thr^{1008} is an indirect target of staurosporine, we determined the transport activity of the corresponding mutants upon application of 8 μM staurosporine. S31A, T34D, and T999D mutants were stimulated by staurosporine to a similar extent as $KCC2^{WT}$ (Fig. 5 and Table 3). In contrast, mutations S31D, T34A, S932A/D, T999A, and T1008A/D abrogated stimulation by staurosporine. These data indicate that all five amino acid residues tested, Ser^{31}, Thr^{34}, Ser^{932}, Thr^{999}, and Thr^{1008}, are involved in the staurosporine-mediated effect.

As described previously, NEM, which generally activates KCCs (27, 57, 58), closely mimics the effect of staurosporine (27). To investigate whether this assumption holds true, we analyzed the impact of NEM on the transport activity of $KCC2^{S31A/D}$, $KCC2^{T34A/D}$, $KCC2^{S728A/D}$, $KCC2^{S932A/D}$, $KCC2^{T999A/D}$, and $KCC2^{T1008A/D}$. As observed for staurosporine, NEM still stimulated transport activity of the mutant T999D and failed to enhance the transport activity of S932D. Contrary to staurosporine, NEM also enhanced the transport activity of S31D, T34A, T932A, T999A, and T1008A/D, whereas it did not affect the transport activity of S31A, T34D, or S932D. Thus, we demonstrate for the first time that staurosporine and NEM can differentially affect KCC2-mediated transport activity.

Discussion

The main function of KCC2 is to establish a low intracellular $[Cl^-]$ as this is required for the hyperpolarizing action of GABA and glycine. Decreased Cl^- extrusion by dysregulated KCC2 activity has been associated with a variety of disorders (12, 18, 19, 23, 25). One potent mechanism to rapidly and reversibly regulate the intrinsic transport rate and cell-surface abundance of KCC2 is phosphorylation and dephosphorylation of serine, threonine, and tyrosine residues (23). Recently, some progress in our understanding of the regulatory impact of specific phosphosites (27, 34, 35, 39, 41, 43) and underlying kinases and phosphates (35–37, 43–46) has been made.

Here, we focused on the functional characterization of *bona fide* phosphorylation sites of KCC2 that were identified by MS analysis of brain tissue. Site-directed mutagenesis in combination with transport activity measurements identified a potent role of Ser^{932} and Thr^{1008} in phosphoregulation. Phosphorylation of Ser^{932} (mimicked by S932D) and dephosphorylation of Thr^{1008} (mimicked by T1008A) increase KCC2 activity. In principle, such an increase can arise from an increased cell-surface abundance of the protein or from an intrinsic conformational change (20, 23). Surface biotinylation experiments demonstrated that surface abundance of S932D and T1008A were indistinguishable from $KCC2^{WT}$. Thus, their increased transport activity resulted from intrinsically kinetic changes. Similar results were reported previously for the mutants T934D and S937D (27).

Ser^{932} is located within exon 22, which is exclusively present in vertebrate KCC2 and nontherian KCC4. This exon also harbors the previously characterized phosphorylation sites Thr^{934}, Ser^{937}, and Ser^{940} (27, 43). Dephosphorylation of Thr^{934} and Ser^{937}, mimicked by mutation to alanine, results in transport activity similar to $KCC2^{WT}$, and phosphorylation of both residues, as mimicked by mutation to aspartate, intrinsically increases KCC2 transport activity (27). Furthermore, PKC-directed phosphorylation of Ser^{940} enhances KCC2 cell-surface stability and increases ion transport, whereas mutation of Ser^{940} to alanine results in transport activity that is equal to or decreased compared with $KCC2^{WT}$ (34, 43, 59). Thus, phosphorylation of each phosphosite so far described in exon 22 stimulates KCC2 function. Exon 22 phosphosites are therefore in strikingly contrast to non-exon 22 phosphosites such as Thr^{906} and Thr^{1006}. The latter two are highly conserved throughout KCCs, and their dephosphorylation increases KCC2 transport activity (27, 34, 37, 39). In addition, Thr^{1008}, analyzed in the present study, that is near Thr^{1006} conforms to this observation as dephosphorylation augments KCC2 activity as well. Thus, KCC2 harbors two main regulatory principles in which phosphorylation of exon 22–specific phosphosites and dephosphorylation of highly conserved KCC phosphosites outside exon 22 increase KCC2 transport activity. Therefore, con-

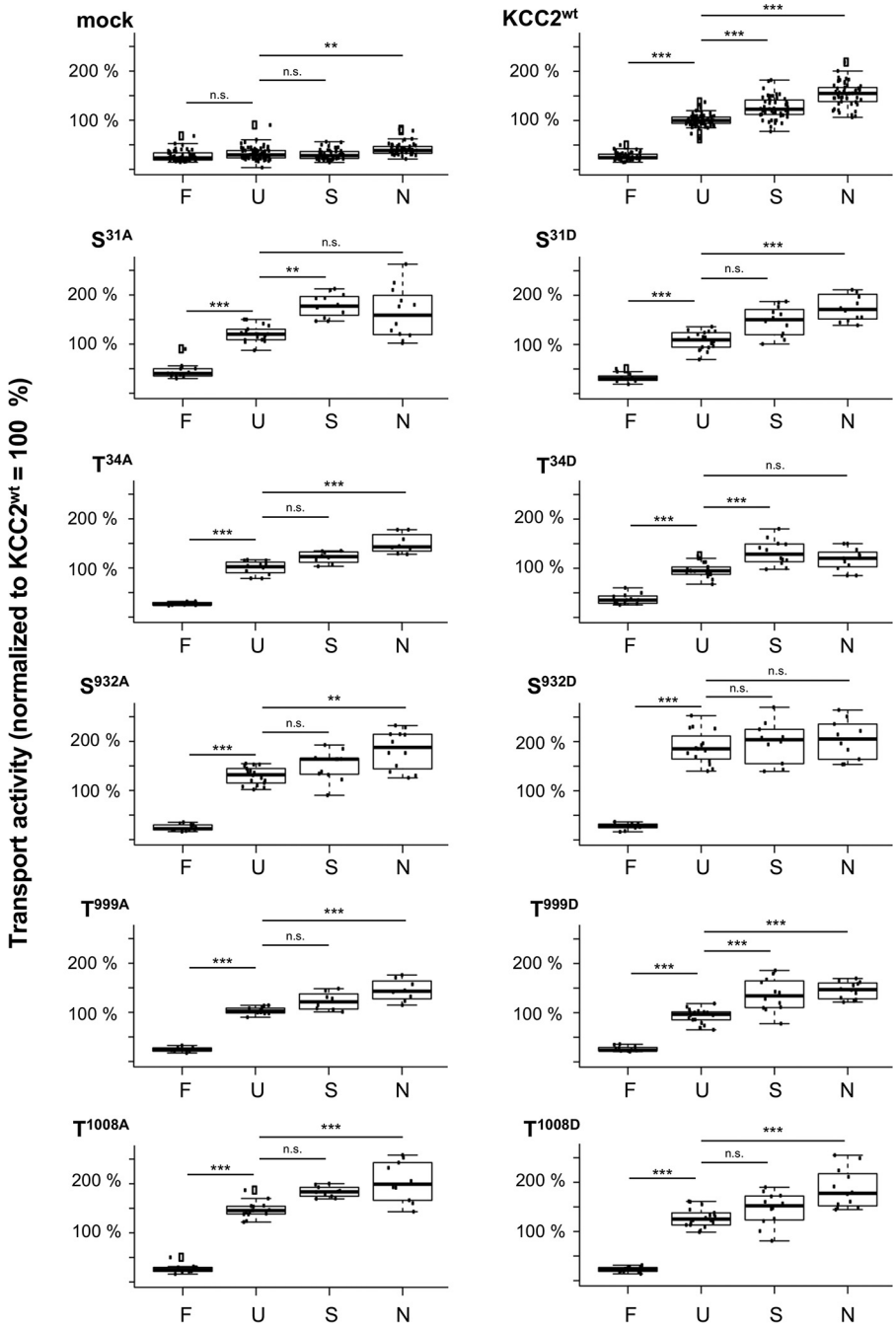

Figure 5. Effect of furosemide, staurosporine, or NEM on transport activity of KCC2 phosphomutants. HEK-293 cells were transfected with $KCC2^{WT}$ or KCC2 phosphomutant constructs. Transport activity was determined by performing Tl^+ flux measurements. Furosemide, staurosporine, or NEM was added 15 min prior to measurement. $KCC2^{WT}$ and all phosphomutants were significantly inhibited by furosemide. $KCC2^{WT}$, $KCC2^{S31A}$, $KCC2^{T34D}$, and $KCC2^{T999D}$ were significantly activated by staurosporine. $KCC2^{WT}$, $KCC2^{S31D}$, $KCC2^{T34A}$, $KCC2^{S932A}$, $KCC2^{T999A/D}$, and $KCC2^{T1008A/D}$ were significantly activated by NEM. The graph represents data of at least four independent measurements (each consisting of two (treated cells) or three (untreated cells) technical replicates) normalized to $KCC2^{WT}$. Statistical analysis is presented in Table 3. **, $p < 0.01$; ***, $p < 0.001$; *n.s.*, not significant. *F*, furosemide; *U*, untreated cells; *S*, staurosporine; *N*, NEM. *Squares* indicate outliers with respect to the 1.5 × interquartile range of the box plot. *Error bars* represent S.E.

trary to other KCC isoforms, which are only up-regulated upon dephosphorylation (39, 60), posttranslational regulation of KCC2 is more complex. This likely equips KCC2 with a more fine-grained phosphoregulatory mechanism as well as an enlarged capacity to integrate multiple signaling cascades compared with other KCC isoforms.

So far, the underlying regulatory mechanisms that lead to phosphorylation and dephosphorylation of specific KCC2 phosphosites have only be partially identified. Ser^{940} is phosphorylated via PKC (43). The phosphosites Thr^{6} of KCC2a and Thr^{906} and Thr^{1006} are regulated by the WNK-SPAK/OSR1 phosphorylation cascade (35–37, 39, 47). Toward the identification of kinases involved in the phosphosites analyzed in this study, we treated HEK-293 cells with staurosporine or NEM. In general, both enhance KCC2 transport activity (27, 28, 56, 61, 62). Recent analyses by Deeb and co-workers (28) demonstrated

Table 3
Transport activity in the presence of staurosporine or NEM
**, $p < 0.01$; ***, $p < 0.001$; n.s., not significant.

	Basal conditions (significance in comparison with $KCC2^{WT}$)	8 μM staurosporine (significance in comparison with untreated samples)	1 mM NEM (significance in comparison with untreated samples)
	%	%	%
Mock	32 ±2 (***)	30 ±2 (n.s.)	41 ±2 (**)
$KCC2^{WT}$	100 ±2 (n.s.)	126 ±4 (***)	153 ±5 (***)
S31A	121 ±7 (n.s.)	179 ±9 (**)	163 ±20 (n.s.)
S31D	108 ±7 (n.s.)	147 ±12 (n.s.)	182 ±18 (***)
T34A	100 ±7 (n.s.)	122 ±6 (n.s.)	150 ±9 (***)
T34D	96 ±6 (n.s.)	132 ±10 (***)	118 ±9 (n.s.)
S932A	130 ±7 (n.s.)	151 ±11 (n.s.)	183 ±15 (**)
S932D	188 ±15 (*)	198 ±18 (n.s.)	204 ±17 (n.s.)
T999A	104 ±4 (n.s.)	123 ±8 (n.s.)	145 ±10 (***)
T999D	93 ±6 (n.s.)	136 ±13 (***)	145 ±7 (***)
T1008A	147 ±7 (**)	184 ±5 (n.s.)	205 ±17 (***)
T1008D	128 ±8 (n.s.)	146 ±13 (n.s.)	187 ±15 (***)

that NEM leads to increased phosphorylation of Ser^{940} and decreased phosphorylation of Thr^{1007} (numbering according to rat KCC2b). The latter might be explained by the observation that NEM also reduces the phosphorylation level of SPAK, which is involved in phosphorylation of Thr^{1007} (28). Interestingly, NEM cannot stimulate the transport activity of T1007E, indicating that the induced activation of KCC2 is mediated by dephosphorylation of Thr^{1007} (28). Here, we show that the phosphomutants S31A, T34D, and S932D also abolish the NEM-mediated increase in KCC2 transport activity. Our results reveal that more than one phosphosite partakes in NEM-induced activation of KCC2.

Previous data indicate that NEM and staurosporine act via the same regulatory mechanism (27). This actually holds true for Thr^{934} and Ser^{937} (27). Our analyses demonstrate for the first time that NEM and staurosporine can differentially impact KCC2 transport activity. NEM did not enhance transport activity of S31A and T34D, whereas staurosporine did not stimulate S31D, T34A, S932A/D, T999A, and T1008A/D. This points to partially different regulatory mechanisms being involved in stimulation of these phosphosites.

Furthermore, two categories of phosphosites were identified. The first category consists of the transport activity–regulatory phosphosites Ser^{932} and Thr^{1008} where mutation to either alanine or aspartate abrogated stimulation by staurosporine. This is expected for a site directly targeted by the staurosporine-mediated action. In line with this result, alteration of the phosphorylation status increased activity (S932D and T1008A). Together, these data strongly suggest that both amino acid residues are *bona fide* target sites of proteins affected by the kinase inhibitor. Additionally, these results reveal that staurosporine acts by triggering both phosphorylation (S932D) and dephosphorylation (T1008A). In the case of Thr^{1008}, this kinase inhibitor might inhibit a kinase that opposes KCC2 activation by phosphorylation of this site. In the case of Ser^{932}, the kinase inhibitor might indirectly inhibit a phosphatase that dephosphorylates this site and thereby opposes KCC2 activation. It is currently unclear why mutation of either site alone abolished significant stimulation by staurosporine. One explanation is a functional cross-talk of both sites. Furthermore, we still noted a trend toward stimulated activity of the single mutants.

The second category consists of Ser^{31} and Thr^{34} for staurosporine and NEM, Thr^{999} for staurosporine, and Ser^{932} for NEM. In these cases, only mutation into one amino acid residue (alanine or aspartate) abrogated stimulation, whereas mutants containing the other amino acid residue replacement were still sensitive to the respective agent. One explanation is that the kind of substitution at these sites defines accessibility to other phosphosites such as Ser^{932} or Thr^{1008} in the case of staurosporine. One conformational state occludes hidden sites (S31A, T34D, and S932D for NEM and S31D, T34A, and T999A for staurosporine), resulting in no further activation of KCC2. The other conformational state deoccludes hidden sites (S31D, T34A, and S932A for NEM and S31A, T34D, and T999D for staurosporine), leading to simulation upon staurosporine or NEM treatment, respectively. Thus, (de)phosphorylation of specific phosphosites likely results in different conformational states of KCC2 termini that have a long-range effect on other phosphosites. They therefore indirectly regulate the transport activity of KCC2. This hypothesis is in line with previous work of Forbush and co-workers (63, 64). They provided evidence that phosphorylation of N-terminal NKCC1 phosphosites leads to movements of transmembrane domains 10 and 12 relative to each other (63, 64). Furthermore, the existence of long-range effects on the phosphostatus of KCC2 is supported by the observation that the mutation R1049C causes a significant >50% decrease in Ser^{940} phosphorylation (11). Full understanding of this issue likely requires the 3D structure of KCC2 to modulate the impact of different phosphosites.

In conclusion, a detailed functional analysis of KCC2 amino acid residues revealed a complex phosphoregulatory landscape. Full understanding of phosphoregulation therefore requires a 3D model of KCC2 and the interacting effectors to simulate the competitive (de)phosphorylation events and the associated conformational changes. In addition, mass spectrometric characterization of KCC2 phosphosites under different treatments would be of advantage. These types of analyses will clarify how single and combined (de)phosphorylation events influence the conformational changes of KCC2 and thus its transport activity. Initial progress toward this goal has been made and revealed a flexible multidomain organization of KCC2 (65). Furthermore, future studies should address the role of phosphosites in KCC2 trafficking. Most studies, including our own, analyze phosphosites in nonneuronal cells with a simplified morphology compared with the high degree of compartmentalization in neurons. The N terminus of KCC2, for instance, is required for

Table 4
Forward primers for site-directed mutagenesis
for, forward.

	Sequence (5′ to 3′)
S31A for	CTTCATCAACGCCACGGACACGG
S31D for	TCCCTTCATCAACGACACGGACACGGAGAAG
T34A for	CAACAGCACGGACGCGGAGAAGGGCAG
T34D for	CTTCATCAACAGCACGGACGATGAGAAGGGCAGAGAGTACG
S932A for	GGAACGGGAGATCCAGGCCATCACAGACGAGTCT
S932D for	GGGAACGGGAGATCCAGGACATCACAGACGAGTCTC
T999A for	GGGGAGAGGGAGGCAGACCCAGAGG
T999D for	CGAGGGGGAGAGGGAGGATGACCCAGAGGTGCATC
T1008A for	AGGTGCATCTTACCTGGGCCAAGGATAAGTCAGTG
T1008D for	GAGGTGCATCTTACCTGGGACAAGGATAAGTCAGTGGC

cell-surface delivery in neurons (66). Interestingly, this part contains various phosphorylation sites with unknown function.

Experimental procedures

Bioinformatics analyses

To identify native phosphosites from proteomics approaches, the two databases PhosphoSitePlus (http://www.phosphosite.org)[3] (52) and PHOSIDA (51) were screened using KCC2 as query. Both databases contained experimentally observed posttranslational modifications obtained by mass spectrometric analyses.

KCC protein sequences for a diverse selection of organisms were obtained from a combination of BLAST searches against GenBank™ and data mining of the Ensembl database and the Joint Genome Institute (http://www.jgi.doe.gov/). The protein sequences of human KCC1 (NP_005063.1), KCC2 (NP_065759.1), KCC3 (NP_598408.1), and KCC4 (NP_006589.2) were used as queries. For each protein in each target species, we saved all sequences with an E-value of at least 10^{-2}. These sequences were then reverse blasted (BLASTp or translated BLAST) against the *Homo sapiens* protein database, and only those protein sequences were retained that showed the same CCC protein sequence of *H. sapiens* that was used as a query sequence as the best hit (E-value of at least 10^{-2}). Each obtained sequence was then aligned at the amino acid level using the default settings in MUSCLE (67) as implemented in SeaView v.4.4.2 (68) and manually improved by eye thereafter.

Construction of expression clones

Site-directed mutagenesis of mouse expression clones for KCC2b (GenBank accession NM_020333.2) was performed according to the QuikChange mutagenesis system (Stratagene, Heidelberg, Germany). Forward oligonucleotides for the generation of the mutations are given in Table 4. Only sequence-verified clones were used for this study.

Cell culture

For immunocytochemistry, K^+-Cl^- cotransporter activity measurements, and cell-surface biotinylation assays, HEK-293 cells were transiently transfected with the respective construct using polyethylenimine (Sigma-Aldrich). 3 h prior to transfection the medium was replaced. Briefly, 400 μl of Dulbecco's modified Eagle's medium (Invitrogen), 18 μl of polyethylenimine, and ~4.5 μg of DNA were mixed and incubated for 15 min at room temperature prior to transfection. For K^+-Cl^- cotransport activity measurements, HEK-293 cells were plated in a 0.1 mg/ml poly-L-lysine–coated 96-black well culture dish (Greiner Bio-One, Frickenhausen, Germany) at a concentration of 100,000 cells/well 24 h after transfection. The remaining cells were plated on a 0.1 mg/ml poly-L-lysine–coated glass coverslip. After ~18 h, coverslips were processed for immunocytochemical analyses to determine transfection rates, which were routinely between 20 and 30% (Fig. S1).

Immunocytochemistry

For immunocytochemistry, all steps were performed at room temperature. HEK-293 cells grown on poly-L-lysine–coated coverslips were fixed for 10 min with 4% paraformaldehyde in 0.2 M phosphate-buffered saline (PBS). After three washing steps in PBS, cells were incubated with blocking solution (2% BSA, 10% goat serum in PBS) for 30 min. Primary antibody solution (anti-KCC2 N1–12; 1:1,000; Neuromab) was added in carrier solution (0.3% Triton X-100, 1% BSA, 1% goat serum in PBS) for 1 h. After washing three times in PBS, the secondary antibody, which was conjugated to a fluorescent probe (Alexa Fluor 488 goat anti-mouse; 1:1,000; Thermo Fisher Scientific, Bremen, Germany), was incubated for 1 h. After three washes in PBS, cells were mounted onto glass slides with Mowiol (Roth, Karlsruhe, Germany) and DAPI (Roth; 1:1000). Photomicrographs were taken using a TCS SP8 confocal laser-scanning microscope (Leica, Wetzlar, Germany).

Determination of K^+-Cl^- cotransport

KCC2 transport activity was determined by Cl^--dependent uptake of Tl^+ in HEK-293 cells as described previously (27, 55, 56). To initiate the flux measurement, the medium in the 96-well culture dish was replaced by 80 μl of preincubation buffer (100 mM *N*-methyl-D-glucamine chloride, 5 mM HEPES, 5 mM KCl, 2 mM $CaCl_2$, 0.8 mM $MgSO_4$, 5 mM glucose, pH 7.4) with 2 μM FlouZin-2 AM dye (Invitrogen) plus 0.2% (w/v) Pluronic F-127 (Invitrogen) and incubated for 48 min at room temperature. Cells were then washed three times with 80 μl of preincubation buffer and incubated for 15 min with 80 μl of preincubation buffer plus 0.1 mM ouabain to block Na^+/K^+-ATPase activity. This was done for three technical replicates for each construct. Afterward, the 96-well plate was placed into a fluorometer (Fluoroskan Accent, Thermo Scientific), and each well was injected with 40 μl of 5× Tl^+ stimulation buffer (12 mM Tl_2SO_4, 100 mM *N*-methyl-D-glucamine chloride, 5 mM HEPES, 2 mM KCl, 2 mM $CaCl_2$, 0.8 mM $MgSO_4$, 5 mM glucose, pH 7.4). Fluorescence was measured in a kinetic-dependent manner (excitation, 485 nm; emission ,538 nm; one frame in 6 s in a 200-s time span) across the entire cell population in a single well. By using linear regression of the initial values of the slope of Tl^+-stimulated fluorescence increase, transport activity was calculated (55, 56).

The effects of the kinase inhibitor staurosporine or NEM were determined by adding 8 μM staurosporine or 1 mM NEM to the preincubation buffer 15 min prior to flux measurement. This was done for two technical replicates for each construct, and at least four independent measurements were performed

[3] Please note that the JBC is not responsible for the long-term archiving and maintenance of this site or any other third party-hosted site.

for each construct. To specifically block transport activity of cation-chloride cotransporters, the loop diuretic furosemide (2 mM) was added to the preincubation buffer. Again, this was done for two technical replicates for each construct, and at least four independent measurements were performed for each construct.

Statistical analyses

Transport activity of each phosphomutant was tested against the control sample (WT), both under control treatment (untreated), using two-sample unequal-variances *t* test after Welch test (69). Because three technical replicates were measured from each independent preparation, we deflated the number of degrees of freedom according to the actual sample size (number of independent preparations) to avoid pseudoreplication. The resulting *p* values were corrected using the Benjamini–Hochberg method (70), which controls the false-discovery rate in multiple comparisons.

For each phosphomutant, we compared the flux measured under four different treatment conditions (untreated, furosemide, staurosporine, and NEM) in a nested analysis of variance where we set the treatment condition as the fixed effect and the replicates as nested random effects. The mixed effects were modeled with the lme function from the R package nlme, and Tukey post hoc analysis was performed with the glht function from the R package multcomp. The *p* values from the post hoc comparisons were adjusted using Holm's sequential Bonferroni correction (71). Note that only *p* values <0.01 were considered to reduce the chances of false positives (type I errors).

Cell-surface biotinylation

KCC2 cell-surface levels were assessed by surface biotinylation as described previously (55, 56). For this purpose, 90–95% confluent 10-cm culture dishes of transfected HEK-293 cells were treated with the membrane-impermeant Sulfo-NHS-SS-Biotin (Thermo Fisher Scientific) according to the provided protocol. After several washes and cell lysis, biotinylated proteins were recovered by a NeutrAvidin-agarose column. After three rounds of washes, biotinylated proteins were eluted in sample buffer. Aliquots of the cell homogenate and of the eluate were collected and analyzed by immunoblot analysis.

To quantify the amount of KCCs expressed at the cell surface, dilution series of each sample were loaded onto a 10% SDS-polyacrylamide gel system. After separation and electrotransfer onto polyvinylidene difluoride membranes, membranes were incubated with N1–12 antibody (1:1,000). After incubation for 2 h at room temperature, membranes were washed four times with TBS-T (20 mM Tris, 150 mM NaCl, 1% Tween, pH 7.5), and the secondary antibody donkey anti-mouse IgG-horseradish peroxidase (Santa Cruz Biotechnology, Heidelberg, Germany) was applied for 2 h. After washing, bound antibodies were detected using an enhanced chemiluminescence assay (GE Healthcare) and a LAS-3000 documentation system (Fujifilm, Düsseldorf, Germany). Quantification of the bands was performed using MultiGauge software V3.1 (Fujifilm). The cell lysate corresponds to the total protein amount and was set to 100%. Only data with recovery values of $100 \pm 20\%$ were included in our analysis. Four to six biological replicas were performed for each construct. Data are given as mean $\pm$ S.D. Significant differences between the groups were analyzed by Student's *t* test.

Author contributions—A. C., W. B., M. W., H. G. N., and A.-M. H. data curation; A. C., W. B., M. W., and A.-M. H. formal analysis; A. C., M. W., H. G. N., and A. M. H. validation; A. C., W. B., and A.-M. H. investigation; A. C. and M. W. visualization; A. C. and A.-M. H. methodology; A. C., H. G. N., and A.-M. H. project administration; A. C., M. W., H. G. N., and A.-M. H. writing-review and editing; H. G. N. and A.-M. H. conceptualization; H. G. N. and A.-M. H. supervision; H. G. N. and A.-M. H. funding acquisition; H. G. N. and A.-M. H. writing-original draft.

Acknowledgment—We thank M. Reents for excellent technical support.

References

1. Blaesse, P., Guillemin, I., Schindler, J., Schweizer, M., Delpire, E., Khiroug, L., Friauf, E., and Nothwang, H. G. (2006) Oligomerization of KCC2 correlates with development of inhibitory neurotransmission. *J. Neurosci.* **26,** 10407–10419 CrossRef Medline
2. Balakrishnan, V., Becker, M., Löhrke, S., Nothwang, H. G., Güresir, E., and Friauf, E. (2003) Expression and function of chloride transporters during development of inhibitory neurotransmission in the auditory brainstem. *J. Neurosci.* **23,** 4134–4145 CrossRef Medline
3. Rivera, C., Voipio, J., Payne, J. A., Ruusuvuori, E., Lahtinen, H., Lamsa, K., Pirvola, U., Saarma, M., and Kaila, K. (1999) The K^+/Cl^- co-transporter KCC2 renders GABA hyperpolarizing during neuronal maturation. *Nature* **397,** 251–255 CrossRef Medline
4. Uvarov, P., Ludwig, A., Markkanen, M., Pruunsild, P., Kaila, K., Delpire, E., Timmusk, T., Rivera, C., and Airaksinen, M. S. (2007) A novel N-terminal isoform of the neuron-specific K-Cl Cotransporter KCC2. *J. Biol. Chem.* **282,** 30570–30576 CrossRef Medline
5. Uvarov, P., Ludwig, A., Markkanen, M., Soni, S., Hübner, C. A., Rivera, C., and Airaksinen, M. S. (2009) Coexpression and heteromerization of two neuronal K-Cl cotransporter isoforms in neonatal brain. *J. Biol. Chem.* **284,** 13696–13704 CrossRef Medline
6. Hübner, C. A., Stein, V., Hermans-Borgmeyer, I., Meyer, T., Ballanyi, K., and Jentsch, T. J. (2001) Disruption of KCC2 reveals an essential role of K-Cl cotransport already in early synaptic inhibition. *Neuron* **30,** 515–524 CrossRef Medline
7. Woo, N.-S., Lu, J., England, R., McClellan, R., Dufour, S., Mount, D. B., Deutch, A. Y., Lovinger, D. M., and Delpire, E. (2002) Hyperexcitability and epilepsy associated with disruption of the mouse neuronal-specific K-Cl cotransporter gene. *Hippocampus* **12,** 258–268 CrossRef Medline
8. Markkanen, M., Karhunen, T., Llano, O., Ludwig, A., Rivera, C., Uvarov, P., and Airaksinen, M. S. (2014) Distribution of neuronal KCC2a and KCC2b isoforms in mouse CNS. *J. Comp. Neurol.* **522,** 1897–1914 CrossRef Medline
9. Kim, J. Y., Liu, C. Y., Zhang, F., Duan, X., Wen, Z., Song, J., Feighery, E., Lu, B., Rujescu, D., St Clair, D., Christian, K., Callicott, J. H., Weinberger, D. R., Song, H., and Ming, G. L. (2012) Interplay between DISC1 and GABA signaling regulates neurogenesis in mice and risk for schizophrenia. *Cell* **148,** 1051–1064 CrossRef Medline
10. Tyzio, R., Nardou, R., Ferrari, D. C., Tsintsadze, T., Shahrokhi, A., Eftekhari, S., Khalilov, I., Tsintsadze, V., Brouchoud, C., Chazal, G., Lemonnier, E., Lozovaya, N., Burnashev, N., and Ben-Ari, Y. (2014) Oxytocin-mediated GABA inhibition during delivery attenuates autism pathogenesis in rodent offspring. *Science* **343,** 675–679 CrossRef Medline
11. Kahle, K. T., Merner, N. D., Friedel, P., Silayeva, L., Liang, B., Khanna, A., Shang, Y., Lachance-Touchette, P., Bourassa, C., Levert, A., Dion, P. A., Walcott, B., Spiegelman, D., Dionne-Laporte, A., and Hodgkinson, A. (2014) Genetically encoded impairment of neuronal KCC2 cotransporter

function in human idiopathic generalized epilepsy. *EMBO Rep.* **15,** 766–774 CrossRef Medline

12. Merner, N. D., Chandler, M. R., Bourassa, C., Liang, B., Khanna, A. R., Dion, P., Rouleau, G. A., and Kahle, K. T. (2015) Regulatory domain or CpG site variation in SLC12A5, encoding the chloride transporter KCC2, in human autism and schizophrenia. *Front. Cell. Neurosci.* **9,** 386CrossRef Medline
13. Huberfeld, G., Wittner, L., Clemenceau, S., Baulac, M., Kaila, K., Miles, R., and Rivera, C. (2007) Perturbed chloride homeostasis and GABAergic signaling in human temporal lobe epilepsy. *J. Neurosci.* **27,** 9866–9873 CrossRef Medline
14. Coull, J. A., Boudreau, D., Bachand, K., Prescott, S. A., Nault, F., Sík, A., De Koninck, P., and De Koninck, Y. (2003) Trans-synaptic shift in anion gradient in spinal lamina I neurons as a mechanism of neuropathic pain. *Nature* **424,** 938–942 CrossRef Medline
15. Rivera, C., Li, H., Thomas-Crusells, J., Lahtinen, H., Viitanen, T., Nanobashvili, A., Kokaia, Z., Airaksinen, M. S., Voipio, J., Kaila, K., and Saarma, M. (2002) BDNF-induced TrkB activation down-regulates the K^+-Cl^- cotransporter KCC2 and impairs neuronal Cl^- extrusion. *J. Cell Biol.* **159,** 747–752 CrossRef Medline
16. Boulenguez, P., Liabeuf, S., Bos, R., Bras, H., Jean-Xavier, C., Brocard, C., Stil, A., Darbon, P., Cattaert, D., Delpire, E., Marsala, M., and Vinay, L. (2010) Down-regulation of the potassium-chloride cotransporter KCC2 contributes to spasticity after spinal cord injury. *Nat. Med.* **16,** 302–307 CrossRef Medline
17. Papp, E., Rivera, C., Kaila, K., and Freund, T. F. (2008) Relationship between neuronal vulnerability and potassium-chloride cotransporter 2 immunoreactivity in hippocampus following transient forebrain ischemia. *Neuroscience* **154,** 677–689 CrossRef Medline
18. Shulga, A., Thomas-Crusells, J., Sigl, T., Blaesse, A., Mestres, P., Meyer, M., Yan, Q., Kaila, K., Saarma, M., Rivera, C., and Giehl, K. M. (2008) Posttraumatic $GABA_A$-mediated $[Ca^{2+}]_i$ increase is essential for the induction of brain-derived neurotrophic factor-dependent survival of mature central neurons. *J. Neurosci.* **28,** 6996–7005 CrossRef Medline
19. Puskarjov, M., Ahmad, F., Khirug, S., Sivakumaran, S., Kaila, K., and Blaesse, P. (2015) BDNF is required for seizure-induced but not developmental up-regulation of KCC2 in the neonatal hippocampus. *Neuropharmacology* **88,** 103–109 CrossRef Medline
20. Medina, I., Friedel, P., Rivera, C., Kahle, K. T., Kourdougli, N., Uvarov, P., and Pellegrino, C. (2014) Current view on the functional regulation of the neuronal K^+-Cl^- cotransporter KCC2. *Front. Cell. Neurosci.* **8,** 27 CrossRef Medline
21. Kahle, K. T., Khanna, A., Clapham, D. E., and Woolf, C. J. (2014) Therapeutic restoration of spinal inhibition via druggable enhancement of potassium-chloride cotransporter KCC2–mediated chloride extrusion in peripheral neuropathic pain. *JAMA Neurol.* **71,** 640–645 CrossRef Medline
22. Alessi, D. R., Zhang, J., Khanna, A., Hochdörfer, T., Shang, Y., and Kahle, K. T. (2014) The WNK-SPAK/OSR1 pathway: master regulator of cation-chloride cotransporters. *Sci. Signal.* **7,** re3-re3 CrossRef Medline
23. Kahle, K. T., Deeb, T. Z., Puskarjov, M., Silayeva, L., Liang, B., Kaila, K., and Moss, S. J. (2013) Modulation of neuronal activity by phosphorylation of the K–Cl cotransporter KCC2. *Trends Neurosci.* **36,** 726–737 CrossRef Medline
24. Gagnon, K. B., and Delpire, E. (2013) Physiology of SLC12 transporters: lessons from inherited human genetic mutations and genetically engineered mouse knockouts. *Am. J. Physiol. Cell Physiol.* **304,** C693–C714 CrossRefMedline
25. Moore, Y. E., Kelley, M. R., Brandon, N. J., Deeb, T. Z., and Moss, S. J. (2017) Seizing control of KCC2: a new therapeutic target for epilepsy. *Trends Neurosci.* **40,** 555–571 CrossRef Medline
26. Khirug, S., Huttu, K., Ludwig, A., Smirnov, S., Voipio, J., Rivera, C., Kaila, K., and Khiroug, L. (2005) Distinct properties of functional KCC2 expression in immature mouse hippocampal neurons in culture and in acute slices. *Eur. J. Neurosci.* **21,** 899–904 CrossRef Medline
27. Weber, M., Hartmann, A.-M., Beyer, T., Ripperger, A., and Nothwang, H. G. (2014) A novel regulatory locus of phosphorylation in the C-terminus of the potassium chloride cotransporter KCC2 that interferes with *N*-ethylmaleimide or staurosporine mediated activation. *J. Biol. Chem.* **289,** 18668–18679 CrossRef Medline
28. Conway, L. C., Cardarelli, R. A., Moore, Y. E., Jones, K., McWilliams, L. J., Baker, D. J., Burnham, M. P., Bürli, R. W., Wang, Q., Brandon, N. J., Moss, S. J., and Deeb, T. Z. (2017) *N*-Ethylmaleimide increases KCC2 cotransporter activity by modulating transporter phosphorylation. *J. Biol. Chem.* **292,** 21253–21263 CrossRef Medline
29. Bize, I., Güvenç, B., Buchbinder, G., and Brugnara, C. (2000) Stimulation of human erythrocyte K-Cl cotransport and protein phosphatase type 2A by N-ethylmaleimide: role of intracellular Mg^{++}. *J. Membr. Biol.* **177,** 159–168 CrossRef Medline
30. Jennings, M. L., and Schulz, R. K. (1991) Okadaic acid inhibition of KCl cotransport. Evidence that protein dephosphorylation is necessary for activation of transport by either cell swelling or N-ethylmaleimide. *J. Gen. Physiol.* **97,** 799–817 CrossRef Medline
31. Song, L., Mercado, A., Vázquez, N., Xie, Q., Desai, R., George, A. L., Jr., Gamba, G., and Mount, D. B. (2002) Molecular, functional, and genomic characterization of human KCC2, the neuronal K-Cl cotransporter. *Mol. Brain Res.* **103,** 91–105 CrossRef Medline
32. Mercado, A., Song, L., Vazquez, N., Mount, D. B., and Gamba, G. (2000) Functional comparison of the K^+-Cl^- cotransporters KCC1 and KCC4. *J. Biol. Chem.* **275,** 30326–30334 CrossRef Medline
33. Hartmann, A.-M., and Nothwang, H. G. (2014) Molecular and evolutionary insights into the structural organization of cation chloride cotransporters. *Front. Cell. Neurosci.* **8,** 470CrossRef Medline
34. Titz, S., Sammler, E. M., and Hormuzdi, S. G. (2015) Could tuning of the inhibitory tone involve graded changes in neuronal chloride transport? *Neuropharmacology* **95,** 321–331 CrossRef Medline
35. Markkanen, M., Ludwig, A., Khirug, S., Pryazhnikov, E., Soni, S., Khiroug, L., Delpire, E., Rivera, C., Airaksinen, M. S., and Uvarov, P. (2017) Implications of the N-terminal heterogeneity for the neuronal K-Cl cotransporter KCC2 function. *Brain Res.* **1675,** 87–101 CrossRef Medline
36. de Los Heros, P., Alessi, D. R., Gourlay, R., Campbell, D. G., Deak, M., Macartney, T. J., Kahle, K. T., and Zhang, J. (2014) The WNK-regulated SPAK/OSR1 kinases directly phosphorylate and inhibit the K^+-Cl^- co-transporters. *Biochem. J.* **458,** 559–573 CrossRef Medline
37. Friedel, P., Kahle, K. T., Zhang, J., Hertz, N., Pisella, L. I., Buhler, E., Schaller, F., Duan, J., Khanna, A. R., Bishop, P. N., Shokat, K. M., and Medina, I. (2015) WNK1-regulated inhibitory phosphorylation of the KCC2 cotransporter maintains the depolarizing action of GABA in immature neurons. *Sci. Signal.* **8,** ra65-ra65 CrossRef Medline
38. Inoue, K., Furukawa, T., Kumada, T., Yamada, J., Wang, T., Inoue, R., and Fukuda, A. (2012) Taurine inhibits K^+-Cl^- cotransporter KCC2 to regulate embryonic Cl^- homeostasis via with-no-lysine (WNK) protein kinase signaling pathway. *J. Biol. Chem.* **287,** 20839–20850 CrossRef Medline
39. Rinehart, J., Maksimova, Y. D., Tanis, J. E., Stone, K. L., Hodson, C. A., Zhang, J., Risinger, M., Pan, W., Wu, D., Colangelo, C. M., Forbush, B., Joiner, C. H., Gulcicek, E. E., Gallagher, P. G., and Lifton, R. P. (2009) Sites of regulated phosphorylation that control K-Cl cotransporter activity. *Cell* **138,** 525–536 CrossRef Medline
40. Lee, H. H., Jurd, R., and Moss, S. J. (2010) Tyrosine phosphorylation regulates the membrane trafficking of the potassium chloride co-transporter KCC2. *Mol. Cell. Neurosci.* **45,** 173–179 CrossRef Medline
41. Strange, K., Singer, T. D., Morrison, R., and Delpire, E. (2000) Dependence of KCC2 K-Cl cotransporter activity on a conserved carboxy terminus tyrosine residue. *Am. J. Physiol. Cell Physiol.* **279,** C860–C867 CrossRef Medline
42. Watanabe, M., Wake, H., Moorhouse, A. J., and Nabekura, J. (2009) Clustering of neuronal K^+-Cl^- cotransporter in lipid rafts by tyrosine phosphorylation. *J. Biol. Chem.* **284,** 27980–27988 CrossRef Medline
43. Lee, H. H., Walker, J. A., Williams, J. R., Goodier, R. J., Payne, J. A., and Moss, S. J. (2007) Direct PKC-dependent phosphorylation regulates the cell surface stability and activity of the potassium chloride cotransporter, KCC2. *J Biol Chem* **282,** 29777–29784 CrossRef Medline
44. Inoue, K., Yamada, J., Ueno, S., and Fukuda, A. (2006) Brain-type creatine kinase activates neuron-specific K^+-Cl^- co-transporter KCC2. *J. Neurochem.* **96,** 598–608 CrossRef Medline

45. Piechotta, K., Garbarini, N., England, R., and Delpire, E. (2003) Characterization of the interaction of stress kinase SPAK with the Na^+-K^+2Cl^- cotransporter in the nervous system. *J. Biol. Chem.* **278,** 52848–52856 CrossRef Medline
46. Piechotta, K., Lu, J., and Delpire, E. (2002) Cation chloride cotransporters interact with the stress-related kinase Ste20-related proline-alanine-rich kinase (SPAK) and oxidative stress response 1 (OSR1). *J. Biol. Chem.* **277,** 50812–50819 CrossRef Medline
47. Heubl, M., Zhang, J., Pressey, J. C., Al Awabdh, S., Renner, M., Gomez-Castro, F., Moutkine, I., Eugène, E., Russeau, M., Kahle, K. T., Poncer, J. C., and Lévi, S. (2017) $GABA_A$ receptor dependent synaptic inhibition rapidly tunes KCC2 activity via the Cl–sensitive WNK1 kinase. *Nat. Commun.* **8,** 1776 CrossRef Medline
48. Vogels, T. P., Sprekeler, H., Zenke, F., Clopath, C., and Gerstner, W. (2011) Inhibitory plasticity balances excitation and inhibition in sensory pathways and memory networks. *Science* **334,** 1569–1573 CrossRef Medline
49. Kopp-Scheinpflug, C., Tozer, A. J., Robinson, S. W., Tempel, B. L., Hennig, M. H., and Forsythe, I. D. (2011) The sound of silence: ionic mechanisms encoding sound termination. *Neuron* **71,** 911–925 CrossRef Medline
50. Woodin, M. A., Ganguly, K., and Poo, M.-M. (2003) Coincident pre- and postsynaptic activity modifies GABAergic synapses by postsynaptic changes in Cl^- transporter activity. *Neuron* **39,** 807–820 CrossRef Medline
51. Gnad, F., Gunawardena, J., and Mann, M. (2011) PHOSIDA 2011: the posttranslational modification database. *Nucleic Acids Res.* **39,** D253–D260 CrossRef Medline
52. Hornbeck, P. V., Kornhauser, J. M., Tkachev, S., Zhang, B., Skrzypek, E., Murray, B., Latham, V., and Sullivan, M. (2012) PhosphoSitePlus: a comprehensive resource for investigating the structure and function of experimentally determined post-translational modifications in man and mouse. *Nucleic Acids Res.* **40,** D261–D270 CrossRef Medline
53. Gillen, C. M., Brill, S., Payne, J. A., and Forbush, B., 3rd (1996) Molecular cloning and functional expression of the K-Cl cotransporter from rabbit, rat, and human. A new member of the cation-chloride cotransporter family. *J. Biol. Chem.* **271,** 16237–16244 CrossRef Medline
54. Culliford, S., Ellory, C., Lang, H.-J., Englert, H., Staines, H., and Wilkins, R. (2003) Specificity of classical and putative Cl-transport inhibitors on membrane transport pathways in human erythrocytes. *Cell. Physiol. Biochem.* **13,** 181–188 CrossRef Medline
55. Hartmann, A.-M., Pisella, L. I., Medina, I., and Nothwang, H. G. (2017) Molecular cloning and biochemical characterization of two cation chloride cotransporter subfamily members of *Hydra vulgaris*. *PLoS One* **12,** e0179968 CrossRef Medline
56. Hartmann, A.-M., Wenz, M., Mercado, A., Störger, C., Mount, D. B., Friauf, E., and Nothwang, H. G. (2010) Differences in the large extracellular loop between the K^+-Cl^- cotransporters KCC2 and KCC4. *J. Biol. Chem.* **285,** 23994–24002 CrossRef Medline
57. Lytle, C., and McManus, T. (2002) Coordinate modulation of Na-K-2Cl cotransport and K-Cl cotransport by cell volume and chloride. *Am. J. Physiol. Cell Physiol.* **283,** C1422–C1431 CrossRefMedline
58. Gagnon, K. B., England, R., and Delpire, E. (2006) Volume sensitivity of cation-Cl^- cotransporter is modulated by the interaction of two kinases: Ste20-related proline-alanine-rich kinase and WNK4. *Am. J. Physiol. Cell Physiol.* **290,** C134–C142 CrossRef Medline
59. Silayeva, L., Deeb, T. Z., Hines, R. M., Kelley, M. R., Munoz, M. B., Lee, H. H., Brandon, N. J., Dunlop, J., Maguire, J., Davies, P. A., and Moss, S. J. (2015) KCC2 activity is critical in limiting the onset and severity of status epilepticus. *Proc. Natl. Acad. Sci. U.S.A.* **112,** 3523–3528 CrossRef Medline
60. Melo, Z., de los Heros, P., Cruz-Rangel, S., Vázquez, N., Bobadilla, N. A., Pasantes-Morales, H., Alessi, D. R., Mercado, A., and Gamba, G. (2013) N-terminal serine dephosphorylation is required for KCC3 cotransporter full activation by cell swelling. *J. Biol. Chem.* **288,** 31468–31476 CrossRef Medline
61. Payne, J. A. (1997) Functional characterization of the neuronal-specific K-Cl cotransporter: implications for $[K^+]_0$ regulation. *Am. J. Physiol. Cell Physiol.* **273,** C1516–C1525 CrossRef
62. Jennings, M. L., and Schulz, R. (1991) Okadaic acid inhibition of KCl cotransporter. *J. Gen. Physiol.* **97,** 799–817 CrossRef Medline
63. Monette, M. Y., and Forbush, B. (2012) Regulatory activation is accompanied by movement in the C terminus of the Na-K-Cl cotransporter (NKCC1). *J. Biol. Chem.* **287,** 2210–2220 CrossRef Medline
64. Monette, M. Y., Somasekharan, S., and Forbush, B. (2014) Molecular motions involved in Na-K-Cl cotransporter-mediated ion transport and transporter activation revealed by internal cross-linking between transmembrane domains 10 and 11/12. *J. Biol. Chem.* **289,** 7569–7579 CrossRef Medline
65. Agez, M., Schultz, P., Medina, I., Baker, D. J., Burnham, M. P., Cardarelli, R. A., Conway, L. C., Garnier, K., Geschwindner, S., Gunnarsson, A., McCall, E. J., Frechard, A., Audebert, S., Deeb, T. Z., and Moss, S. J. (2017) Molecular architecture of potassium chloride co-transporter KCC2. *Sci. Rep.* **7,** 16452 CrossRef Medline
66. Friedel, P., Ludwig, A., Pellegrino, C., Agez, M., Jawhari, A., Rivera, C., and Medina, I. (2017) A novel view on the role of intracellular tails in surface delivery of the potassium-chloride cotransporter KCC2. *eNeuro* **4,** ENEURO.0055–0017.2017 CrossRef Medline
67. Edgar, R. C. (2004) MUSCLE: multiple sequence alignment with high accuracy and high throughput. *Nucleic Acids Res.* **32,** 1792–1797 CrossRef Medline
68. Gouy, M., Guindon, S., and Gascuel, O. (2010) SeaView version 4: a multiplatform graphical user interface for sequence alignment and phylogenetic tree building. *Mol. Biol. Evol.* **27,** 221–224 CrossRef Medline
69. Welch, B. L. (1947) The generalization of student's problem when several different population variances are involved. *Biometrika* **34,** 28–35 Medline
70. Benjamini, Y., and Hochberg, Y. (1995) Controlling the false discovery rate: a practical and powerful approach to multiple testing. *J. R. Stat. Soc. Series B Stat. Methodol.* **57,** 289–300
71. Holm, S. (1979) A simple sequentially rejective multiple test procedure. *Scand. J. Stat.* **6,** 65–70
72. Bergeron, M. J., Gagnon, E., Caron, L., and Isenring, P. (2006) Identification of key functional domains in the C terminus of the K^+-Cl^- cotransporters. *J. Biol. Chem.* **281,** 15959–15969 CrossRef Medline